Published in final edited form as:

Ann Anat. 2017 March ; 210: 135–146. doi:10.1016/j.aanat.2016.11.015.

Aberrant lung remodeling in a mouse model of surfactant dysregulation induced by modulation of the *Abca3* gene☆

Michael F. Beers[a], **Lars Knudsen**[b,c], **Yaniv Tomer**[a], **Julian Maronn**[b], **Ming Zhao**[a], **Matthias Ochs**[b,c,d], and **Surafel Mulugeta**[a,*]

[a]Pulmonary, Allergy, and Critical Care Division, Department of Medicine, University of Pennsylvania, Perelman School of Medicine, Philadelphia, PA, United States

[b]Institute of Functional and Applied Anatomy, Hannover Medical School, Hannover, Germany

[c]Biomedical Research in End-stage and Obstructive Lung Disease Hannover (BREATH), Member of the German Center for Lung Research (DZL), Hannover, Germany

[d]REBIRTH Cluster of Excellence, Hannover, Germany

Abstract

The lipid transporter, ATP binding cassette class A3 (ABCA3), plays a critical role in the biogenesis of alveolar type 2 (AT2) cell lamellar bodies (LBs). A relatively large number of mutations in the *ABCA3* gene have been identified in association with diffuse parenchymal lung disease (DPLD), the most common of which is a missense mutation (valine substitution for lysine at residue 292 (ABCA3^{E292V})) that leads to functional impairment of the transporter *in vitro*. The consequences of *ABCA3*^{E292V} gene expression *in vivo* are unknown. To address this question, we developed mouse models expressing ABCA3^{E292V} knocked-in to the endogenous mouse locus. The parental (F1) mouse line (*mAbca3*^{E292V}) that retained an intronic *pgk-Neo* selection cassette (inserted in reverse orientation) *(mAbca3*^{E292V}*–rNeo)* demonstrated an allele dependent extracellular surfactant phospholipid (PL) deficiency. We hypothesize that this PL deficiency leads to aberrant parenchymal remodeling contributing to the pathophysiology of the DPLD phenotype. Compared to wild type littermates, baseline studies of mice homozygous for the *pgk-Neo* insert (*mAbca3*^{E292V}*–rNeo*$^{+/+}$) revealed nearly 50% reduction in bronchoalveolar lavage (BAL) PL content that was accompanied by quantitative reduction in AT2 LB size with a compensatory increase in LB number. The phenotypic alteration in surfactant lipid homeostasis resulted in an early macrophage predominant alveolitis which peaked at 8 weeks of age. This was followed by age-dependent development of histological DPLD characterized initially by peribronchial inflammatory cell infiltration and culminating in both an emphysema-like phenotype (which included stereologically quantifiable reductions in both alveolar septal surface area and volume of septal wall tissue) plus foci of trichrome-positive collagen deposition together with substantial proliferation of hyperplastic AT2 cells. In addition to spontaneous lung remodeling, *mABCA3*^{E292V}*–rNeo* mice were rendered more vulnerable to exogenous injury. Three weeks

☆This paper belongs to the special issue surfactants and surface activity.

*Corresponding author at: Pulmonary, Allergy, and Critical Care Division, University of Pennsylvania, Perelman School of Medicine, Surfactant Biology Laboratories, Edward J. Stemmler Hall, Suite 218, 3450 Hamilton Walk, Philadelphia, PA 19104, United States. Fax: +1 215 746 0376. mulugeta@mail.med.upenn.edu1 (S. Mulugeta).

following intratracheal bleomycin challenge, *mAbca3–rNeo* mice demonstrated allele-dependent susceptibility to bleomycin including enhanced weight loss, augmented airspace destruction, and increased fibrosis. Removal of the *rNeo* cassette from *mAbca3* alleles resulted in restoration of BAL PL content to wild-type levels and an absence of changes in lung histology up to 32 weeks of age. These results support the importance of surfactant PL homeostasis as a susceptibility factor for both intrinsic and exogenously induced lung injury/remodeling.

Keywords

Pulmonary; Surfactant; Phospholipids; ABCA3; Lung disease; Lamellar bodies; Pathogenesis

1. Introduction

The ATP binding cassette class A, member 3 (ABCA3) glycoprotein is part of a highly conserved multispan transmembrane ABC superfamily of transporters that uses the energy of ATP hydrolysis to translocate a variety of substrates, ranging from ions to large molecules, across extra- and intracellular membranes. The human *ABCA3* gene has been mapped to chromosome 16p13.3 and encodes a 1704-amino acid protein (Connors et al., 1997). Structure prediction algorithms suggest that ABCA3 is typical of most ABC transporters, consisting of two tandemly linked functional units (Higgins et al., 1986). Two transmembrane domains (six α-helices per domain) form the conduit through which substrates cross the membrane. These domains also contain substrate-binding sites, which contribute to transport specificity. Two ATP binding cassettes (ABC1 and ABC2) (nucleotide binding domains) couple the energy of ATP hydrolysis for substrate translocation. Although the ABCA3 transporter is found in many tissues, it is highly expressed in the alveolar type 2 (AT2) cells predominantly localized at the limiting membrane of the lamellar body (LB) (Mulugeta et al., 2002; Yamano et al., 2001). Studies suggest that ABCA3 functions as an intracellular transporter of cholesterol and phospholipids including phosphatidylcholine (PC), phosphatidylglycerol (PG), phosphatidylserine (PS), and sphingomyelin (SM) (Cheong et al., 2006, 2007; Ban et al., 2007; Fitzgerald et al., 2007). Additionally, in both *Abca3* knockout mouse models and human *ABCA3* null patients, this transporter (along with surfactant protein B) has been recognized as one of the critical regulators of LB biogenesis (Ban et al., 2007; Bullard et al., 2005; Cheong et al., 2007; Fitzgerald et al., 2007).

Diffuse parenchymal lung diseases (DPLDs) represent a heterogeneous group of progressive disorders that affect the distal pulmonary interstitium and conducting airways. Well summarized in recent consensus statements (Travis et al., 2013; Antoniou et al., 2014) in brief, the clinical, radiographic, physiologic, and pathologic presentations of DPLD are diverse; however, a number of common features support the inclusion of a variety of endophenotypes in this larger disease category umbrella. In most of these, the disease is believed to be triggered by epithelial dysfunction that participates in an abnormal healing response ultimately leading to scar formation, organ malfunction, gas exchange impairment, and respiratory failure. Over half a million people were affected by DPLD worldwide in 2013, causing over 400 thousand deaths (GBD 2013 Mortality and Causes of Death

Collaborators, 2015). In adults, idiopathic pulmonary fibrosis (IPF), one of the most common subtypes of DPLD of unknown etiology, affects over 5 million people globally and typically results in a need for lung transplantation or in death within 2–5 years of diagnosis (Raghu et al., 2011). An important DPLD endophenotype has recently emerged in which the histology and pathology reflect elements of both fibrotic and emphysema-like remodeling (Jankowich and Rounds, 2012). Additionally, familial forms of pulmonary fibrosis can also be present in children and are part of the larger spectrum of childhood interstitial lung disease (chILD) (Kitazawa and Kure, 2015). The partially defined pathogenesis of IPF (and chILD) has been a major obstacle in developing effective therapies capable of stabilizing or improving lung function in these disorders.

The importance of ABCA3 to surfactant homeostasis and overall lung health is underscored by various features found in association with lung disorders linked to mutations in the *ABCA3* gene. Over 150 sporadic and familial mutations consisting of homozygous, missense, nonsense, and frameshift mutations, as well as heterozygous insertion and splice-site mutations, have been identified. In new borns, *ABCA3* null phenotypes (=Type 0 mutants) present with fatal respiratory failure accompanied by clinical and radiological findings consistent with perinatal surfactant deficiency (Wert et al., 2009; Shulenin et al., 2004; Carrera et al., 2014). Moreover, small, markedly abnormal LBs containing electron dense inclusion bodies have been observed by electron microscopy in the AT2 cells of lung tissue from patients carrying nonsense, missense, and splice-site mutations in the *ABCA3* (Shulenin et al., 2004; Tryka et al., 2000; Wert et al., 2009). These key features, including neonatal lethality, atelectatic respiratory failure, loss of mature LBs, and a dramatic reduction in levels of surfactant phospholipid species have also been observed in *Abca3* null mouse models (Cheong et al., 2007; Fitzgerald et al., 2007; Ban et al., 2007).

In contrast to the initial description of *ABCA3* null gene mutations in newborns with severe surfactant deficiency, both mis-folded/ER retained (=Type I) or functionally impaired (=Type II or hypomorphic) mutant *ABCA3* alleles can be found in older children and adults with histological features of DPLD and IPF (Bullard et al., 2005; Bullard and Nogee, 2007; Doan et al., 2008; Bissler et al., 2008). It has become increasingly evident that there are additional *cis*- and *trans*-allelic mutations within *ABCA3* gene that can act as disease modifiers (Bullard and Nogee, 2007; Kitazawa et al., 2013; Flamein et al., 2012; Goncalves et al., 2014; Beers and Mulugeta, 2016). Several reports have identified patients suffering from chronic lung disorders (with diagnoses of various types of DPLD including pulmonary fibrosis) that carry compound heterozygous mutations (Bullard et al., 2005; Bullard and Nogee, 2007; Kitazawa et al., 2013; Flamein et al., 2012) or an accompanying *SFTPC* mutation mutations (Bullard and Nogee, 2007; Crossno et al., 2010). These findings suggest that while one mutation may not cause a phenotype or may present with a milder lung disease, a secondary *in trans ABCA3* alteration or a mutation in another gene may influence the severity of the disease.

The effects of altered surfactant component metabolism on lung repair/remodeling is incompletely described, although mice constitutively deficient in surfactant protein C (SP-C) or rendered post-natally *mAbca3* null each develop spontaneous emphysemalike remodeling (Glasser et al., 2003; Besnard et al., 2010). Additionally, each of these strains was rendered

more susceptible to exogenous challenges including viral infection (Glasser et al., 2009) and bleomycin (Lawson et al., 2005) with SP-C deficiency and hyperoxia- and mechanical ventilation-induced lung injury (Herber-Jonat et al., 2013) with ABCA3 deficiency. To further address this, we recently developed a knock-in (KI) mouse model carrying the most common DPLD associated mutation (ABCA3 valine for lysine missense mutation at residue 292 (E292V)). *In vitro* studies have shown that the ABCA3^{E292V} is functionally deficient exhibiting moderately compromised ATP binding and lipid transport activities (40% of wild-type activity) (Matsumura et al., 2008). During the course of developing and characterizing this *in vivo* model, we noted that the retention of an intronic, phosphoglycerate kinase I-neomycin *(pgk-Neo)* selection cassette (inserted in reverse orientation) within *mAbca3*^{E292V} mutant alleles (see Fig. 1A) results in a significant, allele-dependent decrease in alveolar surfactant pool sizes. Therefore, we sought to prove the hypothesis that this surfactant deficiency induces an aberrant parenchymal remodeling and contributes to the pathophysiology of the DPLD phenotype. Our investigation documented, a time dependent spontaneous DPLD phenotype characterized by cellular alveolitis, changes in LB morphology. This fundamental difference in surfactant PLs could be corrected by genetic excision of the *pgk-Neo* cassette with the resultant strain resistant to spontaneous histological remodeling for up to 32 weeks. Our results support a specific contribution of the PL component of surfactant in aberrant lung injury/repair/remodeling.

2. Materials and methods

2.1. Generation of mouse pgk-Neo-Abca3-E292V mutant targeting vector

Targeting vector construction: Construction of targeting vector was performed by Gene Bridges Company (Heidelberg, Germany) using a recombineering-based strategy (Liu et al., 2003). Briefly, the bacterial artificial chromosome (BAC)-encoded fragment of interest from a murine C57BL/6 strain was retrieved and subcloned into a minimal pMV vector (gap repair). Synthesis of a mini targeting vector was performed that contained a DNA fragment carrying the E292V point mutation flanked by appropriate targeting arms and *FRT-pgk-gb2-Neo/km-FRT* cassette. The FRT-flanked *pgk-Neo* cassette together with the point mutation was then inserted into the *mAbca3* locus of the corresponding subclone by one Red/ET step (triple recombination). Finally, the functional regions (FRT, point mutation, restriction sites, and resistant cassette) were verified by sequencing.

2.2. Production of the Abca3^{E292V}–rNeo mouse line

Using this vector, a series of *Abca3*^{E292V} mouse lines were generated in collaboration with the University of Pennsylvania Gene Targeting Core and Transgenic and Chimeric Mouse Facility. Briefly, the targeting vector was linearized by using unique NotI and SacII sites and electroporated into C57BL/6 mouse embryonic stem (ES) cells. Following G418 selection, surviving colonies were picked and screened for homologous recombination using a primer specific for the targeted allele. The presence of the targeted allele was confirmed by Southern blot hybridization in eleven clones. Two targeted ES cell clones containing the *pgk-Neo* cassette together with the E292V mutation were injected into blastocysts of Balb/c mice and transferred to pseudopregnant females. Chimeric offspring were crossed with C57BL/6 mice and offspring were screened for germ line transmission by coat color, PCR,

and Southern blot hybridization. The F1 generation, containing the *pgk-Neo* cassette (inserted in reverse orientations), was designated as $Abca3^{V}$–*rNeo*$^{+}$.

Removal of the *pgk-Neo* cassette was accomplished by cross breeding the $Abca3^{E292V}$–*rNeo* mouse line with transgenic C57BL/6J mice constitutively expressing an enhanced variant of *Saccharomyces cerevisiae FLP1* recombinase (FlpE) (Jackson laboratory, Bar Harbor, ME). The resultant *pgk-Neo* cassette excised mouse line was designated as $Abca3^{V}$–(*rNeo*$^{-}$).

All protocols were reviewed and approved by the Institutional Animal Care and Use Committees of the University of Pennsylvania and adhered to the principles of the National Institutes of Health Guide for the Care and Use of Laboratory Animals.

2.3. Bronchoalveolar lavage (BAL) analysis

BAL was collected from mice by gently lavaging five times with 1 ml sterile saline. Processing and analysis of BAL has been described previously (Jain et al., 2007). Briefly, cell pellets obtained by centrifuging BAL samples at 400 × *g* for 10 min were resuspended in 1 ml of PBS, and total cell counts were determined using a Z1 Coulter Counter (Beckman-Coulter, Indianapolis, IN). Cytospins from BAL were prepared and stained with Diff-Quik for microscopic analysis.

Total protein content of BAL was determined by the Bradford method with bovine IgG as a standard (Bradford, 1976). Total lipids were extracted from whole BAL supernatant with chloroform-methanol as described previously (Bligh and Dyer, 1959). Total phospholipid content was determined by Bartlett's colorimetric estimation of inorganic phosphorus (Bartlett, 1959).

Immunoblotting of BAL was performed according to the previously described procedure (Mulugeta et al., 2005) using successive incubations with primary polyclonal anti-SP-B (PT3) (Ross Laboratories, Columbus, OH), 1:3000, followed by goat anti-rabbit horseradish peroxidase conjugated secondary antibody (1:10,000). Bands were visualized by enhanced chemiluminescence using a commercially available kit (ECL Western blotting detection reagents; Amersham, Arlington Heights, IL). Chemiluminescent images were produced either by exposure to film or by direct acquisition using the Kodak 440 imaging system (New Haven, CT).

2.4. Quantitative real-time polymerase chain reaction

Total lung RNA was purified with TRIzol Reagent (Thermo-Fisher Scientific). cDNA was prepared using the RetroScriopt Kit (Ambion, Thermo-Fisher Scientific) and quantitative singleplex polymerase chain reaction (PCR) was performed using an ABI Prism 7900 system (Applied Biosystem). TaqMan assays and primers (Applied Biosystem) for exons 25–27 (Cat. #: 4331182) and exons 11–13 (Cat. # 4351372) were used. Results are depicted as relative quantities of RNA after correcting for 18S followed by normalizing to wild type controls.

2.5. Lung preparation for stereological examination

At the age of 32 weeks, whole lungs were fixed by tracheal instillation with a constant pressure of 25 cm H_2O, applying a 1.5% glutaraldehyde/1.5% paraformaldehyde mixture in 0.15 M HEPES buffer and further processed for design-based stereology (Muhlfeld and Ochs, 2013). After determination of lung volumes (V(lung)) using fluid displacement and measurement of resulting buoyancy forces as previously described (Scherle, 1970), complete lungs were subjected to a systematic uniform random sampling procedure for light and electron microscopy as described elsewhere (Tschanz et al., 2014) and sampled tissue was embedded in Technovit 8100 (Heraeus Kulzer, Wehrheim, Germany) or Epon, respectively. For light microscopy, single sections were stained with toluidine blue. Epon embedded tissue was cut for assessment with the physical dissector. The first and the fourth of a consecutive row of 1 μm thick semithin sections were mounted on one slide and stained with toluidine blue so that the distance from the top of the first to the fourth section was 3 μm. Finally, two consecutive ultrathin sections of 80 nm thickness were placed on one grid representing a dissector pair for counting of lamellar bodies at the electron microscopic level.

2.6. Stereological analysis

Stereological assessment is based on the ATS/ERS statement on quantitative evaluation of lung structure (Hsia et al., 2010; Knudsen et al., 2014). To quantify phenotypic changes, surface area of alveolar epithelium (S(alvepi,lung)), volumes of alveolar septal wall (V(sep,lung)) and acinar airspaces composed of alveolar (V(alv,lung)) and ductal (V(duct,lung)) were determined by point and intersection counting (Ochs and Muhlfeld, 2013; Muhlfeld and Ochs, 2013). Within the reference space the volume fractions (V_V) and surface area density (S_V) of the structures of interest were quantified and multiplied with the reference space (*e.g.* lung volume) to obtain absolute data per lung. Using the physical dissector in combination with the rotator-method the total number (N(AT2,lung)) per lung as well as the number-weighted mean volume of AT2 cells were quantified (Knudsen et al., 2011). At electron microscopic level, the intracellular surfactant pool, defined as the total volume of lamellar bodies (LB) within AT2 cells (V(LB,AT2)), was assessed by point counting and the number of LB per AT2 cell (N(LB,AT2)) was determined using the physical dissector (Knudsen et al., 2011). The number-weighted mean volume of LB ((v_N(LB)) was calculated by dividing the V(LB,AT2) and N(LB,AT2).

2.7. Immunohistochemistry

Immunochemical staining of paraffin-embedded lung sections was performed as previously described (Brasch et al., 2002). Following the removal of paraffin, samples were incubated with anti-NPRO (polyclonal antisera raised against the Met [10]-Glu [23] domain of rat proSP-C recognizes the N-terminal flanking peptide of human proSP-C) at 1:200 dilution. Texas Red- conjugated secondary goat anti-rabbit IgG polyclonal antibody (Jackson Immunoresearch Laboratories, West Grove, PA) at 1:200 dilution were used for visualization. Fluorescence images of air-dried and Mowiol mounted slides were viewed on an Olympus I-70 inverted fluorescent microscope (Olympus, Melville, NY). Fluorescence images were captured using a Hamamatsu 12-bit coupled-charged device camera

(Hamamatsu, Hamamatsu, Japan). Image processing was performed using Metamorph, Version 7.8.4.0 Software (Universal Imaging, West Chester, PA).

2.8. Bleomycin injury model

Mice (12–15 weeks old) were anesthetized with intraperitoneal injection of pentobarbital sodium (70 mg/kg) and suspended by their front teeth from an elastic band attached on an angled plexiglass stand. The tongue was gently lifted with forceps and an otoscope was inserted toward the larynx to allow an unobstructed view of the vocal folds. 50 μl of bleomycin (1 or 2U/kg as indicated in figure legend) solution was administered via an insulin syringe fitted with PE-10 tubing, followed by 100 μl air. The mice were observed following the procedure to ensure they recovered completely from anesthesia. At designated time points following bleomycin administration, mice were euthanized by pentobarbital injection. Lungs were harvested and prepared for histological examination.

2.9. Statistics

To assess differences between groups, analyses were performed with GraphPad Instat (GraphPad Software, San Diego, CA) using a one-way analysis of variance with the Tukey-Kramer post hoc test (P values <0.05 were considered significant). Results are presented as the mean ± SEM unless otherwise indicated.

3. Results

3.1. Aberrant surfactant phospholipid pool size develops in mABCA^{E292V}–rNeo-mice

The F1 generation of the *Abca3*^{E292V} mouse model harbored an intronic insertion of the *FRT-pgk-gb2- Neo/km-FRT* cassette upstream from exon 9 together with E292V point mutation knocked into exon 9 of the *mAbca3* locus (Fig. 1A). Litter size was normal with balanced gender distribution and pups appeared healthy with the expected Mendelian patterns of gene transmission of the FRT-flanked *pgk-Neo* cassette (reversely oriented) *mAbca3-E292V (mAbca3*^{E292V}*–rNeo)* knock in (KI) gene. Mice survived into adulthood without overt signs of respiratory distress. Consistent with a loss of function, analysis of total phospholipid (PL) content of bronchoalveolar lavage (BAL) from these mice revealed allele dependent diminution of total PL levels compared to wild type (WT) control (Fig. 1B). BAL phospholipids were approximately three-quarters (76%) and nearly half (57%) of the WT PL level in heterozygous *mAbca3*^{E292V}*–rNeo* (*mAbca3*^{E292V}*–rNeo*$^{+/-}$) and homozygous *mAbca3*^{E292V}*–rNeo (mAbca3*^{E292V}*–rNeo*$^{+/+}$ mice), respectively. These low levels of surfactant PLs were sustained at all time points examined including 8, 12 (data not shown), and 16 (Fig. 1B) wk old mice.

To determine the specificity of ABCA3 induced changes in surfactant, steady state SP-B content in the BAL of these mice was assessed by Western blotting (Fig. 1C). The unaltered SP-B content in *mAbca3*^{E292V}*–rNeo*$^{+}$ mice compared to wild type mice is consistent with the concept that lower PL level observed in the *mAbca3*^{E292V}*–rNeo*$^{+}$ mice is a product of an inherent decline in AT2 cell PL content and not due to decreased/aberrant overall secretion by AT2 cells.

The decrease in surfactant phospholipid levels in *mAbca3*^{E292V}*–rNeo*$^{+}$ mice was accompanied by an increase in mABCA3 expression. Using Real-Time Quantitative PCR, we noted a significant increase in *mAbca3* message level in *mAbca3*^{E292V}*–rNeo*$^{+/+}$ mouse lungs compared to WT, *or mAbca3*^{E292V}*–rNeo*$^{+/-}$, mice (Fig. 1D); however, this was insufficient to rescue the PL deficiency. This decrease in surfactant PL levels in the face of increased *mAbca3* mRNA suggests an additional effect of the *rNeo* cassette on mutant mABCA3 protein production. However, the lack of a reliable mABCA3 antibody for immunoblot use has precluded comprehensive evaluation of mABCA3 protein levels in the lungs of these mice. Furthermore and consistent with this concept, the genetic removal of the *Neo* cassette restored surfactant homeostasis. That is, crossing the *mAbca3*^{E292V}*–rNeo*$^{+}$ line with a constitutively active FLP-E deleter mouse line (Fig. S1A) to produce *Abca3*^{V}*–(rNeo*$^{-}$*)* mice restored surfactant PL content (Fig. S1B) that cannot be accounted for by increases in *mAbca3* mRNA (Fig. S1C). These results indicate that although the intrinsic functional transporter activity is markedly impaired by this mABCA3^{E292V} mutation *in vitro* (Matsumura et al., 2008), the mE292V mouse has developed some additional compensatory mechanisms (*e.g.* surfactant PL secretion, recycling, or degradation) to maintain surfactant PL levels and is the subject of a separate study. The remainder of the current study leverages the observed changes in *mAbca3*^{E292V}*–rNeo*$^{+}$ mice to characterize the contribution of chronic surfactant PL insufficiency on lung parenchymal homeostasis.

3.2. Pgk-Neo insertion in mAbca3 gene disrupts intracellular surfactant homeostasis in AT2 cells

Lamellar bodies represent the principal storage pool for intracellular surfactant. Electron microscopic evaluation of AT2 cell ultrastructure revealed dramatic changes induced by *ABCA3*^{E292V}*–rNeo* expression. In contrast to WT, abnormally small LBs were readily apparent at 32 weeks in *mAbca3*^{E292V}*–rNeo*$^{+/+}$ mice (Fig. 2A). Supporting this observation, stereological analysis revealed allelic-dependent reduction in the mean volume of LBs in *mAbca3*^{E292V}*–rNeo*$^{+}$ mice (Fig. 2B) and this phenomenon correlated inversely with LB number (Fig. 2C) suggesting a compensatory mechanism to counter balance the reduced LB size in AT2 cells. Additional stereological measurements at baseline did not show significant differences between sample groups in the size (Fig. 2D) and number (Fig. 2E) of AT2 cells (Table S1).

3.3. mAbca3^{E292V}–rNeo^{+} surfactant deficient mice demonstrate increased cell counts

Total BAL cell counts were obtained at 4, 8, 16, and 32 weeks post natal age of individual mice (Fig. 3A). While WT animals showed relatively stable BAL cell numbers, a moderately severe alveolitis developed in *mAbca3*^{E292V}*–rNeo* animals with total cell counts peaking at 8 weeks of age in *mAbca3*^{E292V}*–rNeo*$^{+/+}$ mice. Evaluation of BAL cytospin preparations indicated that this was a monocyte/macrophage predominant population (Fig. S2). Early in the course, large foamy activated macrophages appeared in both *mAbca3*^{E292V}*–rNeo*$^{+/-}$ and *mAbca3*^{E292V}*–rNeo*$^{+/+}$ mice at 8 weeks which were replaced at later time points by increasing numbers of monocytes (arrowheads) and neutrophils (arrows).

3.4. mAbca3^{E292V}–rNeo mice demonstrate parenchymal inflammatory cell infiltration and alveolar remodeling

The early changes in BAL surfactant phospholipid content, BAL cell counts, and total protein in *mAbca3*^{E292V}*–rNeo*$^{+/+}$ animals were accompanied by subsequent, significant, and age dependent alterations in lung morphology. At 6 weeks, lungs of homozygous *mAbca3*^{E292V}*–rNeo*$^{+/+}$ mice exhibited an increased pleiotropic inflammatory cell infiltration consisting of leukocytes and macrophages primarily in a peribronchial distribution (Fig. 4A, arrow). This was followed by a spatially heterogeneous disruption of distal lung architecture evident at 32 weeks in *mAbca3*^{E292V}*–rNeo*$^{+/+}$ mice (Fig. 4B and C). Areas of thinning alveolar septal walls as well as marked enlargement of the alveolar airspace were prominent (Figs. 4B and S3) in these lungs, in combination with increased incidence of intra-alveolar (Fig. S4), but primarily peribronchial leukocyte and macrophage infiltrates (Fig. 4B, arrow). In addition to these changes, we also noted a patchy fibrotic remodeling pattern in many lobes consisting of trichrome positive regions denoting dense collagen deposition and medial thickening accompanied by AT2 cell hyperplasia (Fig. 4D) and a persistence of bimodal populations of both normal sized and abnormally large macrophages (Fig. 4C, arrows and Fig. S2).

Because of the spatially heterogeneous nature of the remodeling, changes in histology were quantified by stereological analysis of Hematoxylin-Eosin stained sections represented in Fig. 4B. Using this unbiased analysis, *mAbca3*^{E292V}*–rNeo*$^{+/+}$ mice demonstrated a significant decrease in surface area of the alveolar septa (Fig. 5A) and reduction in septal wall tissue volume (Fig. 5B) consistent with the observed emphysema-like lung remodeling seen in aged cohorts. No significant differences were observed between the genotypes in several other parameters measured including volumes of lung parenchyma, alveoli, alveolar epithelium, and ductal airspace along with overall lung volume and mean septal thickness (Table S2). The fibrotic component characterized by septal wall thickening showed intra-individual but also inter-individual variability of a very heterogeneous distribution such that the emphysema-like phenotype dominates the stereological parameters without an increase in septal wall thickness as one would expect to be found in view of the focal septal wall thickening seen in Fig. 4C.

3.5. Injury/repair dysregulation in the surfactant deficient mAbca3^{E292V}–rNeo^{+} lung

Since surfactant PL deficiency or migration of inflammatory cells into the alveoli did not appear to alter the alveolar structure of young *mAbca3*^{E292V}*–rNeo* mice, we hypothesized that chronic surfactant deficiency predisposes the alveoli to abnormal injury and repair processes induced by age and would also enhance the propensity of these mice to develop aberrant repair responses to exogenous “second hits”. To address this, we used intratracheal (IT) instillation of bleomycin, a commonly used model of experimental lung fibrosis (Phan and Kunkel, 1992; Zhang et al., 1994; Lawson et al., 2005; Degryse et al., 2010), to examine lung response to sub acute oxidative stress in *mAbca3*^{E292V}*–rNeo*$^{+}$ mice. As demonstrated in Fig. 6A, there was significant allelic-dependent morbidity in IT bleomycin treated (2U/kg) *mAbca3*^{E292V}*–rNeo*$^{+}$ mice. Consistent with this finding, Trichrome-stained lung sections of 12 week old *mAbca3*^{E292V}*–rNeo*$^{+}$ mice 21 days after 1 U/kg bleomycin instillation demonstrated a gradient of augmented airspace destruction and fibrosis (Fig. 6B).

4. Discussion

The effect of altered surfactant phospholipid metabolism and its distinct influence on the pathogenesis of DPLD is often underappreciated because attention is frequently focused on the primary source, the AT2 cells. Accordingly, altered surfactant homeostasis is commonly considered an inevitable consequence secondary to AT2 cell dysregulation and injury. Here we show that intronic insertion of a reversely inserted, non-expressing *Neo* cassette in the *mAbca3* gene results in a reduction of surfactant PL level in a dose-dependent manner. Although this mouse model has an *mABCA3–E292V* mutation that has been shown to disrupt the transporter's function, our study demonstrates that the marked PL deficiency is independent of this mutation and is a direct consequence of the intronic *Neo* cassette (Fig. 1E). While the *E292V* mutation is likely to modify the disease course in this mouse model, the decrease in surfactant PL appears to directly influence early stage (as early as 8 weeks) inflammatory cell infiltration and late stage profound disruption of lung architecture with the phenotype characteristics of DPLD and emphysema. Our study further suggests that chronic surfactant PL deficiency renders the lung vulnerable to second hits that may lead to fibrotic lung remodeling.

Under baseline conditions, altered levels of total PL (Fig. 1B) appear to underlie the primary basis for the age-dependent aberrant lung injury/remodeling mechanism in the $mAbca3^{E292V}$–$rNeo^{+}$ mice. While younger $mAbca3^{E292V}$–$rNeo^{+}$ mice have shown increases in inflammatory cells (Fig. 3A and B) without any apparent disruption of alveolar structure (Fig. 4A), older mice exhibited patchy but consistent alteration of alveolar morphology comprising of collagen deposition, AT2 cell hyperplasia (Fig. 4D) infiltrated by both normal size and abnormally large macrophages (Fig. 4B and C), and a decrease in alveolar septal surface and septal wall tissue (Fig. 5 and Table S2). It is now well established that pulmonary surfactant is essential for alveolar stability and in reducing the alveolar surface tension during the respiratory cycle and its alteration is a common contributing factor for disorders such as respiratory distress syndrome, pulmonary alveolar proteinosis, and DPLD (Akella and Deshpande, 2013). The inflammatory cell infiltration in the context of surfactant insufficiency, observed in the 8 week old $mAbca3^{E292V}$–$rNeo^{+}$ mouse lung suggests the initiation of an aberrant alveolar injury/repair cycle. The aberrant alveolar repair in turn can induce the release of inflammatory mediators to further alter the composition and function of surfactant PL including its immunosuppressive properties (discussed below) to undergo inappropriate lung remodeling ultimately leading to lung disease (Hamm et al., 1992; Akella and Deshpande, 2013) at a later stage in the mouse life.

The significantly elevated level of alveolar inflammatory cells (Fig. 3A), comprising macrophages, monocytes, and neutrophils (Figs. 3B and S2), in the $mAbca3^{E292V}$–$rNeo^{+}$ mice suggests a functional role for normal surfactant PLs in suppressing immunoreactivity. Notwithstanding the contribution of surfactant proteins including surfactant protein-(SP) A, SP-D, and to a lesser degree SP-C in pulmonary immunity (Kishore et al., 2006; Mulugeta and Beers, 2006), the PL component of surfactant has been shown to suppress the inflammatory response. Kerecman and his colleagues have demonstrated that SP-A- and SP-D-free exogenous surfactant PLs inhibit proinflammatory cytokines of alveolar macrophage (Kerecman et al., 2008). Surfactant PLs including phosphatidylglycerol (PG) and

phosphatidylinositol (PI) have anti-inflammatory properties (Kuronuma et al., 2009) and the presence of high concentrations of PG reduces the number of macrophages in the alveolar space (Poelma et al., 2005). The major component of PLs, phosphatidylcholine (PC), mediates the interaction between macrophages and lymphocytes and may contribute to the regulation of lymphocyte proliferation (Nishiyama-Naruke and Curi, 2000). The PL components of surfactant such as PC, PG, and PI have also been shown to suppress the activation and proliferative response of lymphocytes (Catanzaro et al., 1988; Wilsher et al., 1988, 1990; Sitrin et al., 1985). This effect of surfactant PL appears to be limited to dormant lymphocytes and during early stages of lymphocyte activation, as activated lymphocytes are unaffected. Moreover, surfactant PL influences a variety of lymphocyte activities including proliferation, differentiation, immunoglobulin synthesis, and natural killer cell activity (Catanzaro et al., 1988; Wilsher et al., 1988, 1990; Sitrin et al., 1985; Baughman and Strohofer, 1989). Together, these studies demonstrate that surfactant PL plays a critical role in protecting the lung not only from atelectasis and subsequent alveolar injury/damage, but also from an improper and disproportionate immune response.

Mechanistically, altered LB homeostasis, together with an apparent inefficient compensatory mechanism, appears to be among the components that contribute to the PL deficiency in *mAbca3*^{E292V}*–rNeo*$^{+}$ mice. Ultrastructural analysis of AT2 cells of these mice revealed abnormally small LBs (Fig. 2B) that are consistent with characteristic LB morphology seen in children with respiratory distress syndrome or fatal respiratory failure carrying many of the *ABCA3* mutations (Shulenin et al., 2004; Bullard et al., 2005; Besnard et al., 2010; Doan et al., 2008). Since the underlying cause of PL deficiency in these mice is the insufficient expression of the mABCA3 transporter and the removal of the *rNeo* cassette restores BAL PL content to normal level, further studies will be necessary to determine the individual contribution of either E2922V mutation or *mAbca3*^{E292V}*–rNeo*$^{-}$ alleles in altering LB structure and surfactant homeostasis. Nevertheless, the presence of increased LB numbers in the face of abnormally small LBs (Fig. 2B and C) in *mAbca3*^{E292V}*–rNeo*$^{+}$ mice implies a counter regulatory system by AT2 cells to compensate for the deficiency of surfactant PL, a phenomenon that is likely to occur in related human lung disorders. Additional compensatory mechanisms by AT2 cells to correct the reduced surfactant PL level in the lung of these mice also includes increased *mAbca3* message levels (Fig. 1D). Together, these data support the concept that surfactant homeostasis is a regulated process that harbors sensory and counter regulatory mechanisms in AT2 cells.

The existence of compensatory mechanisms to restore surfactant homeostasis in response to mABCA3 deficiency is supported by previous studies utilizing conditional deletion of the *mAbca3* gene in a mouse model (Besnard et al., 2010). The majority of mice in which the *mAbca3* gene has been conditionally deleted (*Abca3*$^{\Delta/\Delta}$) from AT2 cells prior to birth died shortly after birth from respiratory distress related to surfactant deficiency. The ~33% that survived developed emphysema without a significant pulmonary inflammation phenotype. However, an interesting characteristic of the surviving mice is that while the overall mechanism of lipid synthesis in the lungs of these mice is disrupted including decreased level of the mABCA3 substrates such as PC and PG and a decline in the levels of transcription factors and mRNAs that are known in the regulation of lung lipid metabolism, the lyso-PC and phosphatidylethanolamine contents were significantly increased.

These compensatory mechanisms may not be limited to PLs, but may also extend to surfactant proteins as mature SP-B secretion appears to be unaltered in the *mAbca3*^{E292V}*–rNeo* mice (Fig. 1C) as opposed to *Abca3* null mice where impaired processing of proSP-B and/or blockage of mature SP-B secretion in near term embryos have been observed (Fitzgerald et al., 2007; Cheong et al., 2007). Indeed, impaired processing of proSP-B and reduced levels of both pro and mature SP-B have also been reported in some patients with *ABCA3* mutations (Brasch et al., 2006; Bullard and Nogee, 2007), suggesting that normal lamellar body formation is required for processing of SP-B. In contrast, while the PL content and composition of the surviving mice of the *Abca3*$^{\Delta/\Delta}$ mice were markedly reduced in lung tissue, LB size and numbers, and BAL fluid, there was no difference in mature SP-B or SP-C expression compared to control mice (Besnard et al., 2010). Taken together, these studies suggest compensatory mechanisms that may play a role in surviving mice/patients of *ABCA3* gene dysregulation-induced PL deficiency. These mechanisms not only are likely to induce enhanced production of PLs but may also improve the processing and secretion efficiency of surfactant proteins such as SP-B and SP-C by AT2 cells.

We have demonstrated an allelic-dependent vulnerability to lung injury as well as an increased propensity to weight loss and a higher morbidity rate in bleomycin treated surfactant deficient mice (Fig. 6) that suggests exogenous stimulants can contribute to disease progression. In response to bleomycin treatment, both *mAbca3*^{E292V}*–rNeo*$^{+/+}$ and *mAbca3*^{E292V}*–rNeo*$^{+/-}$ dose-dependent morbidity indicating a scope of severity that might extend to a total failure of lung function (Fig. 6A). Likewise, *mAbca3*^{E292V}*–rNeo*$^{+/-}$ mice had more extensive lung fibrosis and increased collagen accumulation than wild type controls (Fig. 6B). Comparable to this, the previously reported ABCA3 haploinsufficient mouse model (*mAbca3*$^{+/-}$) (Cheong et al., 2007; Fitzgerald et al., 2007; Ban et al., 2007), with a characteristic phenotype of decreased lung PL levels and decreased lung compliance, has been shown to exhibit susceptibilities to hyperoxia- and mechanical ventilation-induced lung injury (Herber-Jonat et al., 2013). Thus, based on similar studies and clinical findings in various reports related to mutations linked to surfactant component genes such as *SFTPC* and *ABCA3*, it is now believed that in addition to genetic background, environmental exposure is regarded as a critical contributor for the variation observed in disease presentations (Bullard et al., 2005; Bullard and Nogee, 2007; Mulugeta et al., 2015; Salerno et al., 2016) and that multiple hits in the form of genetic modifiers and/or environmental factors are considered to be necessary for augmenting disease severity or even for inducing lung pathology (Bullard and Nogee, 2007; Phan and Kunkel, 1992; Zhang et al., 1994; Lawson et al., 2005; Degryse et al., 2010).

The overall phenotype of the *mAbca3*^{E292V}*–rNeo*$^{+}$ mouse model compared to the *mAbca3*$^{+/-}$ haploinsufficient mice (Cheong et al., 2007; Fitzgerald et al., 2007; Ban et al., 2007) suggests a modifying influence by the *E292V* mutant allele. Although there are some similarities between the two mouse models in terms of both models expressing reduced levels of phospholipids, they exhibit marked baseline phenotypic differences suggesting a role for the E292V mutation to further disrupt AT2 cell homeostasis and consequently to alter lung phenotype. While the homozygous *Abca3* knockout (*mAbca3*$^{-/-}$) mice die from respiratory distress due to surfactant deficiency soon after birth, the *mAbca3*$^{+/-}$ mice survive into adulthood. An apparent reduction in surfactant PLs, due to ABCA3 deficiency,

including PC, PG, PE, and PS typically characterizes this *mAbca3*$^{+/-}$ mouse. However, in contrast to the *mAbca3*^{E292V}*–rNeo*$^{+}$ mouse model that is characterized by early onset of inflammatory response, no significant pulmonary inflammation has been reported in any of the three *mAbca3*$^{+/-}$ mice generated to date (Cheong et al., 2007; Fitzgerald et al., 2007; Ban et al., 2007). At the ultrastructural level, unlike the *mAbca3*^{E292V}*–rNeo*$^{+}$ mice that exhibit smaller size and increased number of LBs (Fig. 2), *mAbca3*$^{+/-}$ mice appear to have a reverse effect exhibiting decreased number of LBs (Cheong et al., 2007) while no changes in LB sizes have been reported. Thus, the variation between the two models supports the concept that mutations in the *mAbca3* gene modify the severity of lung phenotype in the *mAbca3*^{E292V}*–rNeo*$^{+}$ mice, similar to those human *ABCA3* mutations that have been considered to play a role as modifier genes by either co-expression with other surfactant component gene mutations such as *SFTPC* mutations (Bullard and Nogee, 2007; Crossno et al., 2010) or expressed in compound heterozygous state (Bullard et al., 2005; Shulenin et al., 2004; Garmany et al., 2006; Doan et al., 2008; Flamein et al., 2012; Beers and Mulugeta, 2016).

Finally, combined pulmonary fibrosis and emphysema-like phenotype that has been observed in the lungs of these mice (Fig. 4) is consistent with recent reports on patients carrying mutations of the *ABCA3* gene. While this pathological coexistence of emphysema and pulmonary fibrosis has been commonly observed in active or former smokers, they are rarely seen in other pulmonary disorders (Jankowich and Rounds, 2012). *ABCA3* mutation-associated combined pulmonary fibrosis and emphysema was first reported in a 41 year old nonsmoker (Epaud et al., 2014). The patient was a compound heterozygous for ABCA3 mutation with E292V variant in one allele and a nonsense mutation producing a null allele in the other. Likewise, a second 8 year old child, also with compound heterozygous mutation with an L34P and a p. F1203_L1204del mutations has been described with a diagnosis of pulmonary fibrosis and emphysema along with pulmonary hypertension (Ota et al., 2016). Taken together, these reports further support the proposal that disruption of the ABCA3 gene can promote an aberrant lung phenotype characterized by both fibrotic and emphysema-like lung remodeling.

In summary, we have demonstrated that surfactant PL deficiency brought about by a *Neo* cassette insert within the intronic region of the *mAbca3* locus leads to a severe lung phenotype that begins with alveolar inflammatory cell infiltration at the early stage of the mouse life followed by aberrant lung remodeling with characteristics of DPLD- and emphysema-like alveolar disruption in older mice. While the mechanism underlying the diminution of BAL PL as related to the contribution of individual lipid and PL species (PC, PG, PS, etc.) as well as ABCA3 protein production in these mice requires further investigation, the current study has further defined the critical role surfactant PLs play in the maintenance of alveolar integrity and in the pathogenesis of lung disorders such as DPLD and emphysema. Investigation of surfactant PL's impact in shaping the health of the pulmonary system such as those described in this report will contribute important information to understanding disease progression and offer further insights regarding specific targets for therapeutic intervention.

Supplementary Material

Refer to Web version on PubMed Central for supplementary material.

Acknowledgments

The authors acknowledge the support provided by the Gene Targeting (Dr. Tobias Rabbe, Director) and the Transgenic and Chimeric Mouse (Dr. Jean Richa, Director) Core Facilities at the University of Pennsylvania in the development of the transgenic mouse models.

Funding

This work is supported by the National Institutes of Health (HL119436 to M. Beers and HL129150 to S. Mulugeta), The Department of Veterans Affairs (VA Merit Award BX001176 to M. Beers), The American Heart Association (13GRNT17070104 to M. Beers) and The National Institute of Environmental Health Sciences of the National Institutes of Health (P30ES013508). M. Beers is the Albert M. Rose Established Investigator of the Pulmonary Fibrosis Foundation.

Appendix A. Supplementary data

Supplementary data associated with this article can be found, in the online version, at http://dx.doi.org/10.1016/j.aanat.2016.11.015.

Abbreviations

PL	phospholipid
ABCA	ATP binding cassette class A
SP-C	surfactant protein C
SFTPC	gene encoding SP-C proprotein
DPLD	diffuse parenchymal lung disease
LB	lamellar body
BAL	bronchoalveolar lavage

References

Akella A, Deshpande SB. Pulmonary surfactants and their role in pathophysiology of lung disorders. Indian J Exp Biol. 2013; 51(1):5–22. [PubMed: 23441475]

Antoniou KM, Margaritopoulos GA, Tomassetti S, Bonella F, Costabel U, Poletti V. Interstitial lung disease. Eur Respir Rev. 2014; 23(131):40–54. [PubMed: 24591661]

Ban N, Matsumura Y, Sakai H, Takanezawa Y, Sasaki M, Arai H, Inagaki N. ABCA3 as a lipid transporter in pulmonary surfactant biogenesis. J Biol Chem. 2007; 282(13):9628–9634. [PubMed: 17267394]

Bartlett GR. Phosphorous assay in column chromatography. J Biol Chem. 1959; 234:466–468. [PubMed: 13641241]

Baughman RP, Strohofer S. Lung derived surface active material (SAM) inhibits natural killer cell tumor cytotoxicity. J Clin Lab Immunol. 1989; 28(2):51–54. [PubMed: 2787406]

Beers, MF., Mulugeta, S. The biology of the ABCA3 lipid transporter in lung health and disease. Cell Tissue Res. 2016. http://dx.doi.org/10.1007/s00441-016-2554-z

Besnard V, Matsuzaki Y, Clark J, Xu Y, Wert SE, Ikegami M, Stahlman MT, Weaver TE, Hunt AN, Postle AD, Whitsett JA. Conditional deletion of Abca3 in alveolar type II cells alters surfactant homeostasis in newborn and adult mice. AJP: Lung Cell Mol Physiol. 2010; 298(5):L646–L659.

Bissler JJ, McCormack FX, Young LR, Elwing JM, Chuck G, Leonard JM, Schmithorst VJ, Laor T, Brody AS, Bean J, Salisbury S, Franz DN. Sirolimus for angiomyolipoma in tuberous sclerosis complex or lymphangioleiomyomatosis. N Engl J Med. 2008; 358(2):140–151. [PubMed: 18184959]

Bligh EG, Dyer WJ. A rapid method of total lipid extraction and purification. Can J Biochem. 1959; 37:911–917. [PubMed: 13671378]

Bradford MM. A rapid and sensitive method for the quantitation of microgram quantities of protein utilizing the principle of protein-dye binding. Ann Biochem. 1976; 72:248–254.

Brasch F, ten Brinke A, Johnen G, Ochs M, Kapp N, Muller KM, Beers MF, Fehrenbach H, Richter J, Batenburg JJ, Buhling F. Involvement of cathepsin H in the processing of the hydrophobic surfactant-associated protein C in type II pneumocytes. Am J Respir Cell Mol Biol. 2002; 26(6): 659–670. [PubMed: 12034564]

Brasch F, Schimanski S, Muhlfeld C, Barlage S, Langmann T, Aslanidis C, Boettcher A, Dada A, Schroten H, Mildenberger E, Prueter E, Ballmann M, Ochs M, Johnen G, Griese M, Schmitz G. Alteration of the pulmonary surfactant system in full-term infants with hereditary ABCA3 deficiency. Am J Respir Crit Care Med. 2006; 174(5):571–580. [PubMed: 16728712]

Bullard JE, Nogee LM. Heterozygosity for ABCA3 mutations modifies the severity of lung disease associated with a surfactant protein C gene (SFTPC) mutation. Pediatr Res. 2007; 62(2):176–179. [PubMed: 17597647]

Bullard JE, Wert SE, Whitsett JA, Dean M, Nogee LM. ABCA3 mutations associated with pediatric interstitial lung disease. Am J Respir Crit Care Med. 2005; 172(8):1026–1031. [PubMed: 15976379]

Carrera P, Ferrari M, Presi S, Ventura L, Vergani B, Lucchini V, Cogo PE, Carnielli VP, Somaschini M, Tagliabue P. Null ABCA3 in humans: large homozygous ABCA3 deletion, correlation to clinical-pathological findings. Pediatr Pulmonol. 2014; 49(3):E116–E120. [PubMed: 24420869]

Catanzaro A, Richman P, Batcher S, Hallman M. Immunomodulation by pulmonary surfactant. J Lab Clin Med. 1988; 112(6):727–734. [PubMed: 3193028]

Cheong N, Madesh M, Gonzales LW, Zhao M, Yu K, Ballard PL, Shuman H. Functional and trafficking defects in ATP binding cassette A3 mutants associated with respiratory distress syndrome. J Biol Chem. 2006; 281(14):9791–9800. [PubMed: 16415354]

Cheong N, Zhang H, Madesh M, Zhao M, Yu K, Dodia C, Fisher AB, Savani RC, Shuman H. ABCA3 is critical for lamellar body biogenesis in vivo. J Biol Chem. 2007; 282(33):23811–23817. [PubMed: 17540762]

Connors TD, Van Raay TJ, Petry LR, Klinger KW, Landes GM, Burn TC. The cloning of a human ABC gene (ABC3) mapping to chromosome 16p13.3. Genomics. 1997; 39(2):231–234. [PubMed: 9027511]

Crossno PF, Polosukhin VV, Blackwell TS, Johnson JE, Markin C, Moore PE, Worrell JA, Stahlman MT, Phillips JA, Loyd JE, Cogan JD, Lawson WE. Identification of early interstitial lung disease in an individual with genetic variations in ABCA3 and SFTPC. Chest. 2010; 137(4):969–973. [PubMed: 20371530]

Degryse AL, Tanjore H, Xu XC, Polosukhin VV, Jones BR, McMahon FB, Gleaves LA, Blackwell TS, Lawson WE. Repetitive intratracheal bleomycin models several features of idiopathic pulmonary fibrosis. AJP: Lung Cell Mol Physiol. 2010; 299(4):L442–L452.

Doan ML, Guillerman RP, Dishop MK, Nogee LM, Langston C, Mallory GB, Sockrider MM, Fan LL. Clinical, radiological and pathological features of ABCA3 mutations in children. Thorax. 2008; 63(4):366–373. [PubMed: 18024538]

Epaud R, Delestrain C, Louha M, Simon S, Fanen P, Tazi A. Combined pulmonary fibrosis and emphysema syndrome associated with ABCA3 mutations Combined pulmonary fibrosis and emphysema syndrome associated with ABCA3 mutations. Eur Respir J. 2014; 43(2):638–641. [PubMed: 24136335]

Fitzgerald ML, Xavier R, Haley KJ, Welti R, Goss JL, Brown CE, Zhuang DZ, Bell SA, Lu N, McKee M, Seed B, Freeman MW. ABCA3 inactivation in mice causes respiratory failure, loss of pulmonary surfactant, and depletion of lung phosphatidylglycerol. J Lipid Res. 2007; 48(3):621–632. [PubMed: 17142808]

Flamein F, Riffault L, Muselet-Charlier C, Pernelle J, Feldmann D, Jonard L, Durand-Schneider AM, Coulomb A, Maurice M, Nogee LM, Lnagaki N, Amselem S, Dubus JC, Rigourd V, Bremont F, Marguet C, Brouard J, de Blic J, Clement A, Epaud R, Guillot L. Molecular and cellular characteristics ofABCA3 mutations associated with diffuse parenchymal lung diseases in children. Hum Mol Genet. 2012; 21(4):765–775. [PubMed: 22068586]

Garmany TH, Moxley MA, White FV, Dean M, Hull WM, Whitsett JA, Nogee LM, Hamvas A. Surfactant composition and function in patients with ABCA3 mutations. Pediatr Res. 2006; 59(6): 801–805. [PubMed: 16641205]

GBD 2013 Mortality and Causes of Death Collaborators. Global, regional, and national age-sex specific all-cause and cause-specific mortality for 240 causes of death, 1990–2013: a systematic analysis for the Global Burden of Disease Study 2013. Lancet. 2015; 385(9963):117–171. [PubMed: 25530442]

Glasser SW, Witt TL, Senft AP, Baatz JE, Folger D, Maxfield MD, Akinbi HT, Newton DA, Prows DR, Korfhagen TR. Surfactant protein C-deficient mice are susceptible to respiratory syncytial virus infection. Am J Physiol Lung Cell Mol Physiol. 2009; 297(1):L64–L72. [PubMed: 19304906]

Glasser SW, Detmer EA, Ikegami M, Na CL, Stahlman MT, Whitsett JA. Pneumonitis and emphysema in SP-C gene targeted mice. J Biol Chem. 2003; 278(16):14291–14298. [PubMed: 12519727]

Goncalves JP, Pinheiro L, Costa M, Silva A, Goncalves A, Pereira A. Novel ABCA3 mutations as a cause of respiratory distress in a term newborn. Gene. 2014; 534(2):417–420. [PubMed: 24269975]

Hamm H, Fabel H, Bartsch W. The surfactant system of the adult lung: physiology and clinical perspectives. Clin lnvestig. 1992; 70(8):637–657.

Herber-Jonat S, Mittal R, Huppmann M, Hammel M, Liebisch G, Yildirim AO, Eickelberg O, Schmitz G, Hrabe de AM, Flemmer AW, Holzinger A. Abca3 haploinsufficiency is a risk factor for lung injury induced by hyperoxia or mechanical ventilation in a murine model. Pediatr Res. 2013; 74(4):384–392. [PubMed: 23881110]

Higgins CF, Hiles ID, Salmond GP, Gill DR, Downie JA, Evans IJ, Holland IB, Gray L, Buckel SD, Bell AW. A family of related ATP-binding subunits coupled to many distinct biological processes in bacteria. Nature. 1986; 323(6087):448–450. [PubMed: 3762694]

Hsia CC, Hyde DM, Ochs M, Weibel ER. An official research policy statement of the American Thoracic Society/European Respiratory Society: standards for quantitative assessment of lung structure. Am J Respir Crit Care Med. 2010; 181(4):394–418. [PubMed: 20130146]

Jain D, Atochina-Vasserman E, Kadire H, Tomer Y, Inch A, Scott P, Savani RC, Gow AJ, Beers MF. SP-D-deficient mice are resistant to hyperoxia. AJP: Lung Cell Mol Physiol. 2007; 292(4):L861–L871.

Jankowich MD, Rounds SL. Combined pulmonary fibrosis and emphysema syndrome: a review. Chest. 2012; 141(1):222–231. [PubMed: 22215830]

Kerecman J, Mustafa SB, Vasquez MM, Dixon PS, Castro R. Immunosuppressive properties of surfactant in alveolar macrophage NR8383. Inflamm Res. 2008; 57(3):118–125. [PubMed: 18369576]

Kishore U, Greenhough TJ, Waters P, Shrive AK, Ghai R, Kamran MF, Bernal AL, Reid KBM, Madan T, Chakraborty T. Surfactant proteins SP-A and SP-D: structure, function and receptors. Mol Immunol. 2006; 43(9):1293–1315. [PubMed: 16213021]

Kitazawa H, Kure S. Interstitial lung disease in childhood: clinical and genetic aspects. Clin Med Insights Circ Respir Pulm Med. 2015; 9(Suppl. 1):57–68. [PubMed: 26512209]

Kitazawa H, Moriya K, Niizuma H, Kawano K, Saito-Nanjo Y, Uchiyama T, Riki-ishi T, Sasahara Y, Sakamoto O, Setoguchi Y, Kure S. Interstitial lung disease in two brothers with novel compound heterozygous ABCA3 mutations. Eur J Pediatr. 2013; 172(7):953–957. [PubMed: 23443156]

Knudsen L, Atochina-Vasserman EN, Guo CJ, Scott PA, Haenni B, Beers MF, Ochs M, Gow AJ. NOS2 is critical to the development of emphysema in Sft pd deficient mice but does not affect surfactan homeostasis. PLoS One. 2014; 9(1):e85722. [PubMed: 24465666]

Knudsen L, Waizy H, Fehrenbach H, Richter J, Wahlers T, Wittwer T, Ochs M. Ultrastructural changes of the intracellular surfactant pool in a rat model of lung transplantation-related events. Respir Res. 2011; 12:79. [PubMed: 21669009]

Kuronuma K, Mitsuzawa H, Takeda K, Nishitani C, Chan ED, Kuroki Y, Nakamura M, Voelker DR. Anionic pulmonary surfactant phospholipids inhibit inflammatory responses from alveolar macrophages and U937 cells by binding the lipopolysaccharide-interacting proteins CD14 and MD-2. J Biol Chem. 2009; 284(38):25488–25500. [PubMed: 19584052]

Lawson WE, Polosukhin VV, Stathopoulos GT, Zoia O, Han W, Lane KB, Li B, Donnelly EF, Holburn GE, Lewis KG, Collins RD, Hull WM, Glasser SW, Whitsett JA, Blackwell TS, Lawson WE, Polosukhin VV, Stathopoulos GT, Zoia O, Han W, Lane KB, Li B, Donnelly EF, Holburn GE, Lewis KG, Collins RD, Hull WM, Glasser SW, Whitsett JA, Blackwell TS. Increased and prolonged pulmonary fibrosis in surfactant protein C-deficient mice following intratracheal bleomycin. Am J Pathol. 2005; 167(5):1267–1277. [PubMed: 16251411]

Liu PT, Jenkins NA, Copeland NG. A highly efficient recombineering-based method for generating conditional knockout mutations. Genome Res. 2003; 13(3):476–484. [PubMed: 12618378]

Matsumura Y, Ban N, Inagaki N. Aberrant catalytic cycle and impaired lipid transport into intracellular vesicles in ABCA3 mutants associated with nonfatal pediatric interstitial lung disease. AJP: Lung Cell Mol Physiol. 2008; 295(4):L698–L707.

Muhlfeld C, Ochs M. Quantitative microscopy of the lung: a problem-based approach. Part 2: stereological parameters and study designs in various diseases of the respiratory tract. Am J physiol Lung Cell Mol Physiol. 2013; 305(3):L205–L221. [PubMed: 23709622]

Mulugeta S, Beers MF. Surfactant protein C: its unique properties and emerging immunomodulatory role in the lung. Microbes Infect. 2006; 8(8):2317–2323. [PubMed: 16782390]

Mulugeta S, Gray JM, Notarfrancesco KL, Gonzales LW, Koval M, Feinstein SI, Ballard PL, Fisher AB, Shuman H. Identification of LBM180, a lamellar body limiting membrane protein of alveolar type II cells, as the ABC transporter protein ABCA3. J Biol Chem. 2002; 277(25):22147–22155. [PubMed: 11940594]

Mulugeta S, Nureki SI, Beers MF. Lost after translation: insights from surfactant for understanding the role of alveolar epithelial dysfunction and cell quality control in fibrotic lung disease. Am J Physiol Lung Cell Mol Physiol. 2015; 309(6):L507–525. [PubMed: 26186947]

Mulugeta S, Nguyen V, Russo SJ, Muniswamy M, Beers MF. A surfactant protein C precursor protein BRICHOS domain mutation causes endoplasmic reticulum stress, proteasome dysfunction, and caspase 3 activation. Am J Respir Cell Mol Biol. 2005; 32(6):521–530. [PubMed: 15778495]

Ochs M, Muhlfeld C. Quantitative microscopy of the lung: a problem-based approach. Part 1: basic principles of lung stereology. Am J Physiol Lung Cell Mol Physiol. 2013; 305(1):L15–L22. [PubMed: 23624789]

Ota C, Kimura M, Kure S. ABCA3 mutations led to pulmonary fibrosis and emphysema with pulmonary hypertension in an 8-year-old girl. Pediatr Pumonol. 2016; 51(6):E21–E23.

Phan SH, Kunkel SL. Lung cytokine production in bleomycin-induced pulmonary fibrosis. Exp Lung Res. 1992; 18(1):29–43. [PubMed: 1374023]

Poelma DL, Lachmann B, Haitsma JJ, Zimmermann LJ, Van Iwaarden JF. Influence of phosphatidylglycerol on the uptake of liposomes by alveolar cells and on lung function. J Appl Physiol (1985). 2005; 98(5):1784–1791. [PubMed: 15661837]

Raghu G, Collard HR, Egan JJ, Martinez FJ, Behr J, Brown KK, Colby TV, Cordier JF, Flaherty KR, Lasky JA, Lynch DA, Ryu JH, Swigris JJ, Wells AU, Ancochea J, Bouros D, Carvalho C, Costabel U, Ebina M, Hansell DM, Johkoh T, Kim DS, King TE Jr, Kondoh Y, Myers J, Muller NL, Nicholson AG, Richeldi L, Selman M, Dudden RF, Griss BS, Protzko SL, Schunemann HJ. An official ATS/ERS/JRS/ALAT statement: idiopathic pulmonary fibrosis: evidence-based guidelines for diagnosis and management. Am J Respir Crit Care Med. 2011; 183(6):788–824. [PubMed: 21471066]

Salerno T, Peca D, Menchini L, Schiavino A, Boldrini R, Esposito F, Danhaive O, Cutrera R. Surfactant Protein C-associated interstitial lung disease; three different phenotypes of the same SFTPC mutation. Ital J Pediatr. 2016; 42:23. [PubMed: 26925580]

Scherle W. A simple method for volumetry of organ in quantitative stereology. Mikroskopie. 1970; 26(1):57–60. [PubMed: 5530651]

Shulenin S, Nogee LM, Annilo T, Wert SE, Whitsett JA, Dean M. ABCA3 gene mutations in newborns with fatal surfactant deficiency. N Engl J Med. 2004; 350(13):1296–1303. [PubMed: 15044640]

Sitrin RG, Ansfield MJ, Kaltreider HB. The effect of pulmonary surface-active material on the generation and expression of murine B- and T-lymphocyte effector functions in vitro. Exp Lung Res. 1985; 9(1–2):85–97. [PubMed: 3877631]

Travis WD, Costabel U, Hansell DM, King TE, Lynch DA, Nicholson AG, Ryerson CJ, Ryu JH, Selman MS, Wells AU, Behr J, Bouros D, Brown KK, Colby TV, Collard HR, Cordeiro CR, Cottin V, Crestani B, Drent M, Dudden RF, Egan J, Flaherty K, Hogaboam C, Inoue Y, Johkoh T, Kim DS, Kitaichi M, Loyd J, Martinez FJ, Myers J, Protzko S, Raghu G, Richeldi L, Sverzellati N, Swigris J, Valeyre D. An Official American Thoracic Society/European Respiratory Society statement: update of the international multidisciplinary classification of the idiopathic interstitial pneumonias. Am J Respir Crit Care Med. 2013; 188(6):733–748. [PubMed: 24032382]

Tryka AF, Wert SE, Mazursky JE, Arrington RW, Nogee LM. Absence of lamellar bodies with accumulation of dense bodies characterizes a novel form of congenital surfactant defect. Pediatr Dev Pathol. 2000; 3(4):335–345. [PubMed: 10890249]

Tschanz S, Schneider JP, Knudsen L. Design-based stereology: planning, volumetry and sampling are crucial steps for a successful study. Ann Anat. 2014; 196(1):3–11. [PubMed: 23769130]

Wert SE, Whitsett JA, Nogee LM. Genetic disorders of surfactant dysfunction. Pediatr Dev Pathol. 2009; 12(4):253–274. [PubMed: 19220077]

Wilsher ML, Hughes DA, Haslam PL. Immunoregulatory properties of pulmonary surfactant: effect of lung lining fluid on proliferation of human blood lymphocytes. Thorax. 1988; 43(5):354–359. [PubMed: 3194863]

Wilsher ML, Parker DJ, Haslam PL. Immunosuppression by pulmonary surfactant: mechanisms of action. Thorax. 1990; 45(1):3–8. [PubMed: 2321174]

Yamano G, Funahashi H, Kawanami O, Zhao LX, Ban N, Uchida Y, Morohoshi T, Ogawa J, Shioda S, Inagaki N. ABCA3 is a lamellar body membrane protein in human lung alveolar type II cells. FEBS Lett. 2001; 508(2):221–225. [PubMed: 11718719]

Zhang K, Rekhter MD, Gordon D, Phan SH. Myofibroblasts and their role in lung collagen gene expression during pulmonary fibrosis. A combined immunohistochemical and in situ hybridization study. Am J Pathol. 1994; 145(1):114–125. [PubMed: 7518191]

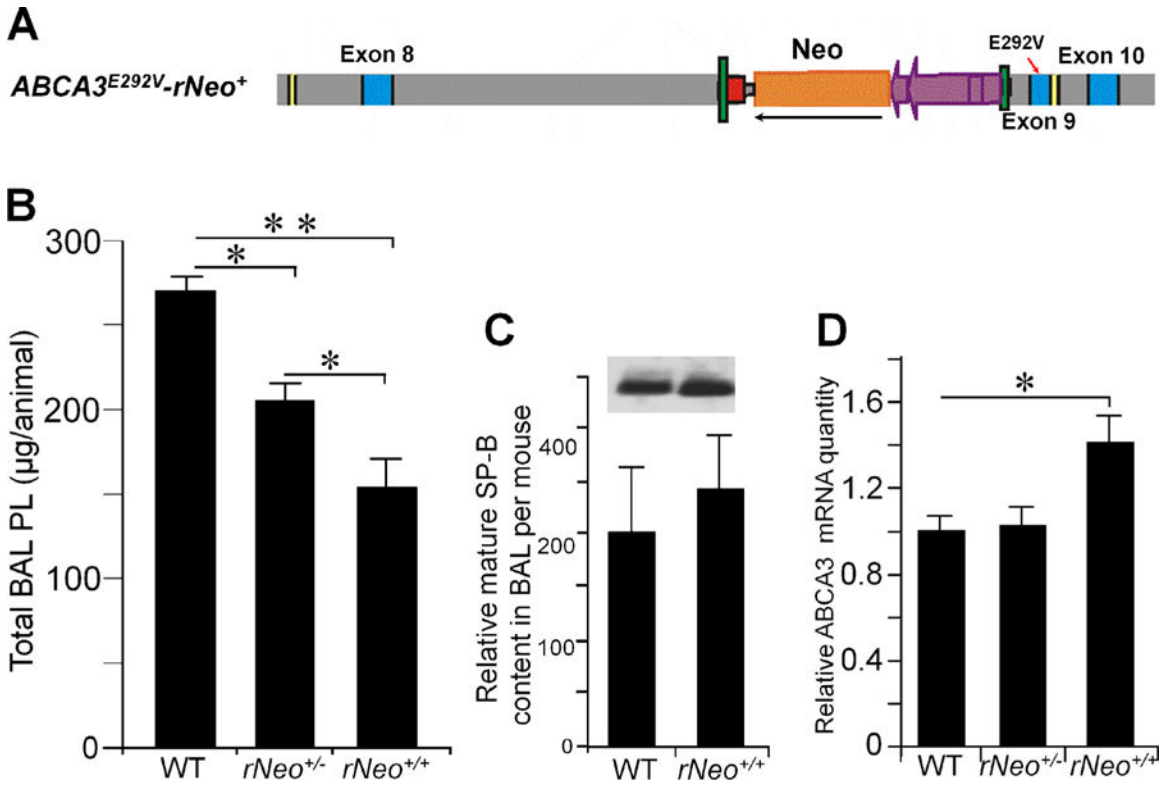

Fig. 1.

(A) Schematic illustration of the *mAbca3*^{E292V}*–rNeo*$^{+}$ mouse model showing the *FRT-pgk-gb2-Neo/km-FRT* cassette insert site within intron 8 in the *Abca3* locus together with the E292V point mutation in Exon 9. (B) Total bronchoalveolar lavage (BAL) phospholipid (PL) content of 16 wk old *mAbca3*^{E292V}*–rNeo*$^{+/-}$, *mAbca3*^{E292V}*–rNeo*$^{+/+}$ mice and WT littermates were measured; *mAbca3*^{E292V}*–rNeo*$^{+/-}$, N = 9; for *mAbca3*^{E292V}*–rNeo*$^{+/+}$, N=10; WT, N = 5. $^{*}P<0.05$, $^{**}P<0.001$. (C, top) Representative immunoblot bands of anti-mature SP-B from BAL of *mAbca3*^{E292V}*–rNeo*$^{+/+}$ *and* WT control mice. (C, bottom) Quantitation of relative intensity of mature SP-B content (as determined by densitometric analysis) from at least 3 mice per group. (D) mRNA levels from *mAbca3*^{E292V}*–rNeo*$^{+/-}$, and *mAbca3*^{E292V}*–rNeo*$^{+/+}$ mice relative to WT *mAbca3* as measured by real time quantitative PCR with at least 5 mice per group. $^{*}P<0.05$, $^{**}P<0.01$.

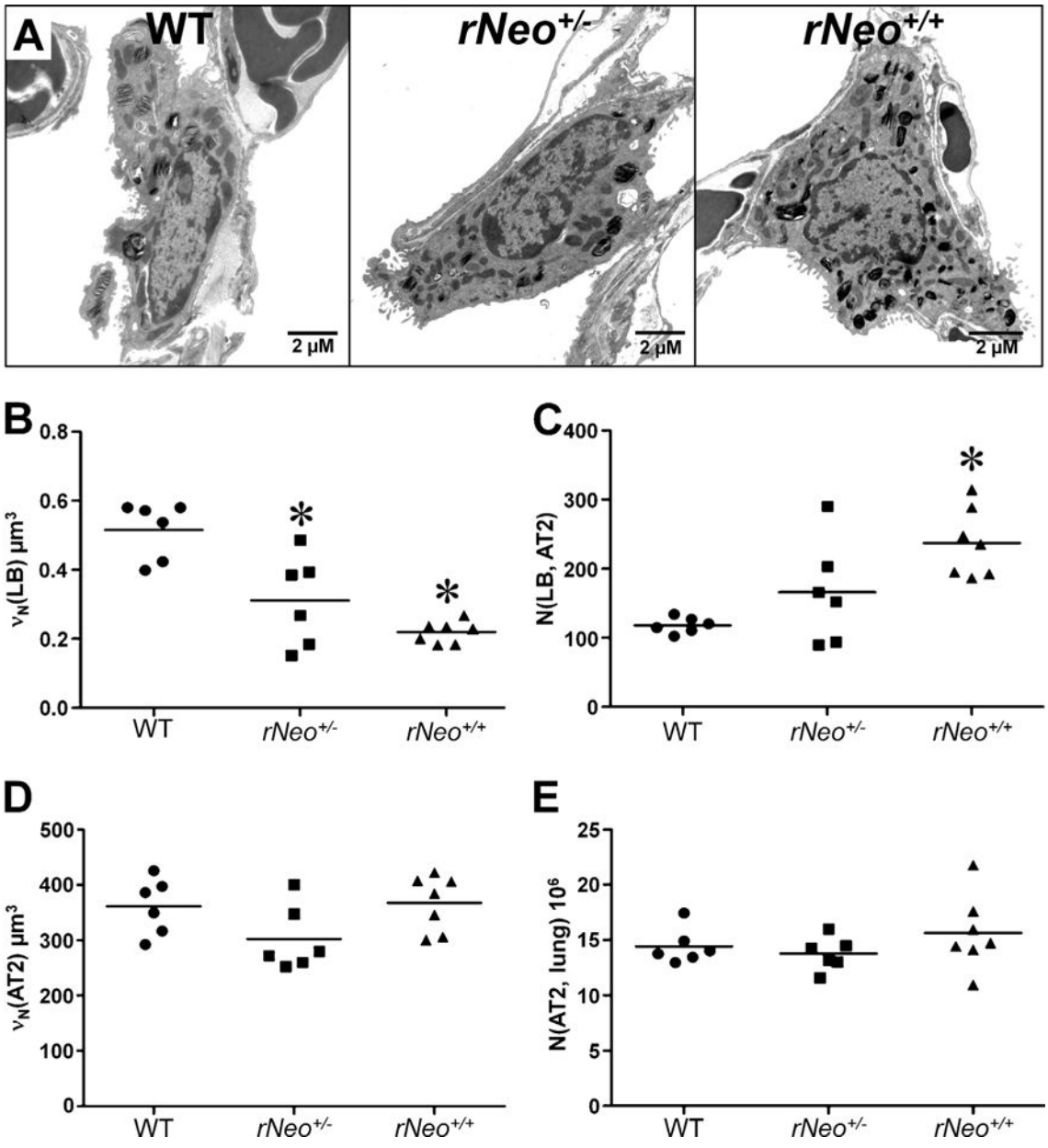

Fig. 2.

(A) Representative electron micrographs of AT2 cells of 32 wk old WT, *mAbca3*^{E292V}–*rNeo*$^{+/-}$, and *mAbca3*^{E292V}–*rNeo*$^{+/+}$ mice. The profiles of AT2 cells in *mAbca3*^{E292V}–*rNeo*$^{+/+}$ mice appear to comprise smaller lamellar bodies compared to WT or *mAbca3*^{E292V}–*rNeo*$^{+/-}$ mice. (B and C) LB size measured as number-weighted mean volume of LB (*vN* (LB) [μm^3]) (B) and number of LBs per AT2 cells (N(LB, AT2)) (B). $^*P<0.05$ *vs* WT. (D and E) AT2 cell size measured as number-weighted mean volume of AT (*vN* (AT2) μm^3) (D) and number of AT2 cells (N(AT2, lung)) 10^6 (E).

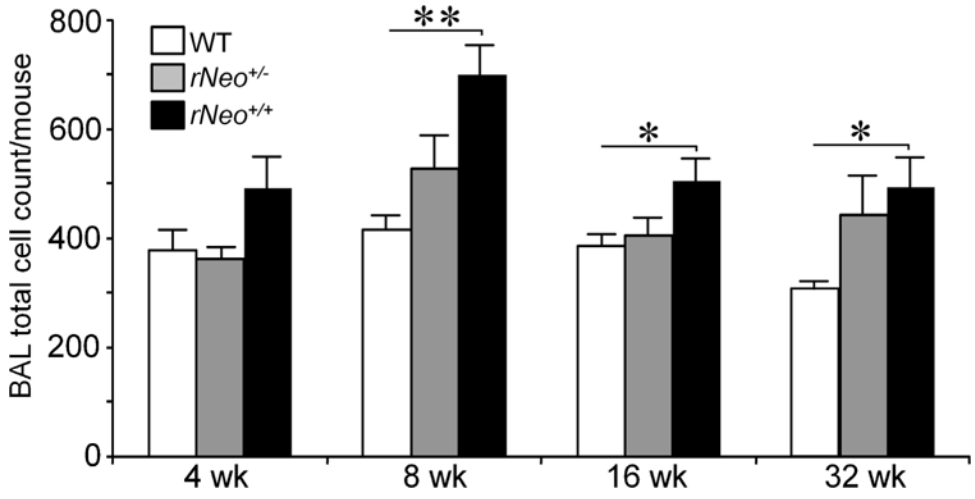

Fig. 3.

BAL total cell counts from 4,8, 16, and 32 wk old *mAbca3*^{E292V}*–rNeo*$^{+/-}$, *mAbca3*^{E292V}*–rNeo*$^{+/+}$ mice and WT control littermates. At least 7 mice per group were used. $^{*}P<0.05$, $^{**}P< 0.005$.

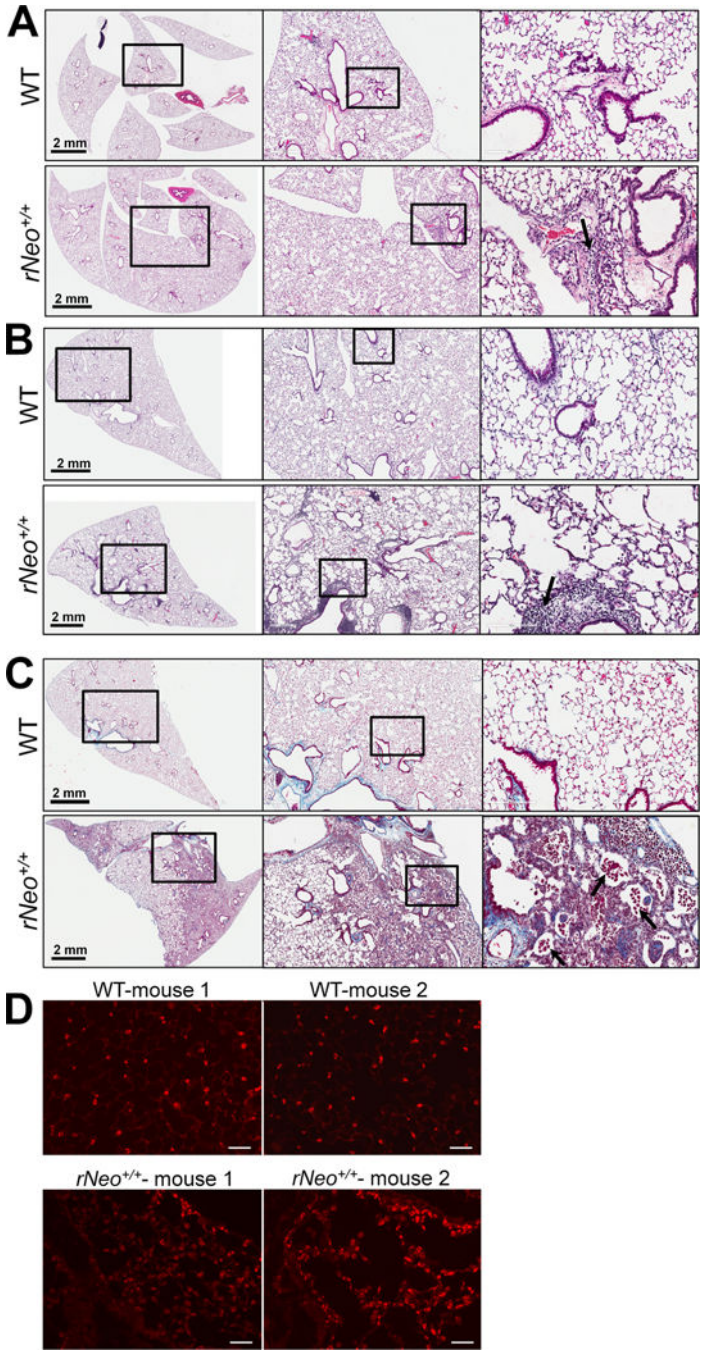

Fig. 4.

(A–C) Representative H&E staining of histological lung sections from 16 (A) and 32 (B and C) wk old *mAbca3*^{E292V}–*rNeo*$^{+/+}$ mice. (A) Moderate inflammatory cell infiltration (arrow) at 16 wk but otherwise normal alveolar structure is exhibited compared to WT littermates. (B) AT 32 wk, common features of the *mAbca3*^{E292V}–*rNeo*$^{+/+}$ mouse lung include patchy but significant perinuclear inflammatory cell infiltration (arrow), thinning of the septal wall, and marked enlargement of the alveolar space. (C) Profound distraction of alveolar architecture detected in 32 wk old *mAbca3*^{E292V}–*rNeo*$^{+/+}$ *mice* comprising areas of dense

collagen deposition, medial thickening populated by an abundance of abnormally large macrophages (arrows). Boxed areas are magnified on the right of each image for better resolution. (D) Representative lung sections from two 32 wk old *mAbca3*^{E292V}*–rNeo*$^{+/+}$ mice and wild type littermates immunostained for Texas Red-conjugated proSP-C antibody (anti-NPRO). Bar, 50 μm.

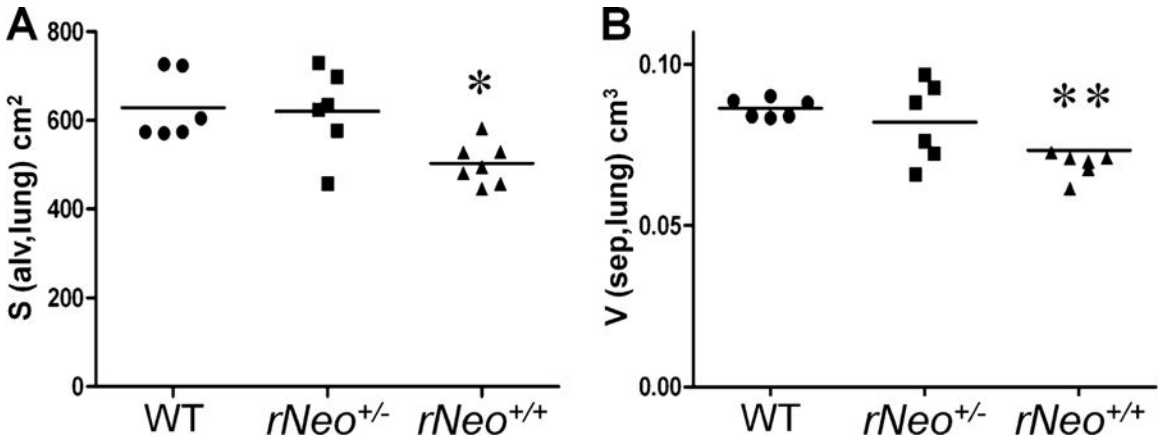

Fig. 5.

Light microscopy-based stereological measurement of lung structure showing decreased surface area of alveolar epithelium (S(salvepi, lung) [cm^2]) (A) and decreased volume of septal wall tissue (V(sep, lung) [mm^3])(B)in *mAbca3*^{E292V}*–rNeo*$^{+/+}$ *mice* compared to *mAbca3*^{E292V}*–rNeo*$^{+/-}$ *mice* and WT littermates. $^{*}P < 0.05$, $^{**}P < 0.001$ *vs* WT.

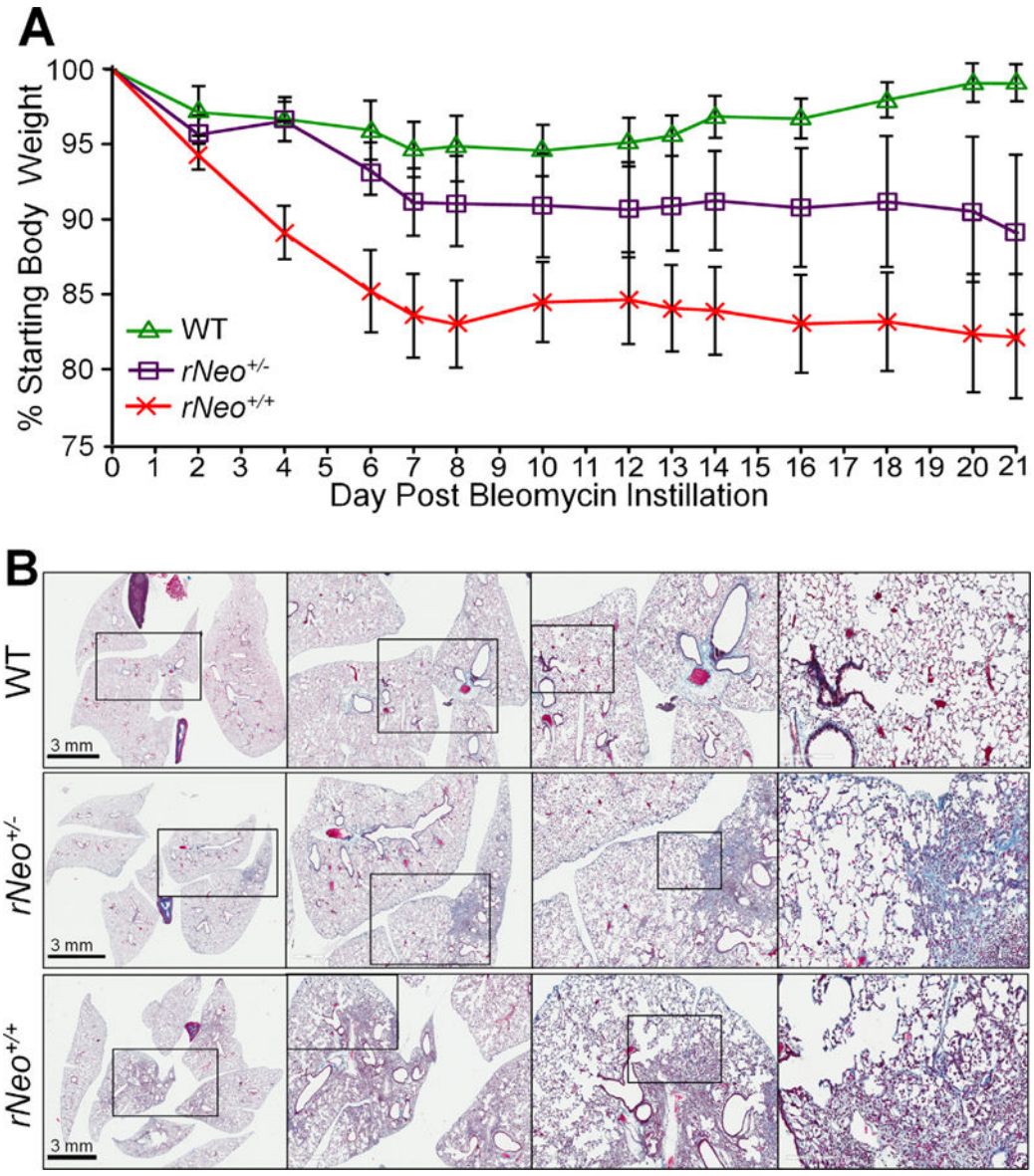

Fig. 6.

(A) Weight-loss in *mAbca3*^{E292V}*–rNeo*$^{+/-}$, *mAbca3*^{E292V}*–rNeo*$^{+/+}$, and WT control mice following IT bleomycin (2U/kg). At least 7 mice per group were used. (B) Representative trichrome staining of histological lung sections from 16 wk old *mAbca3*^{E292V}*–rNeo*$^{+/-}$, *mAbca3*^{E292V}*–rNeo*$^{+/+}$, mice and WT littermates 21 days post intratracheal (IT) bleomycin (1U/kg). Patchy areas of fibrosis were noted in WT and *mAbca3*^{E292V}*–rNeo*$^{+/-}$ mice. In contrast, trichrome stain was more prominent in *mAbca3*^{E292V}*–rNeo*$^{+/+}$ mice displaying severe alveolar destruction and subpleural fibrosis enveloping several lobes. Boxed areas are magnified on the right of each image for better resolution.